Aggregation of red blood cells in suspension: study by light-scattering technique at small angles

Cristian V. L. Pop
Silvia Neamtu
National Institute for Research and Development of Isotopic and Molecular Technologies
Molecular and Biomolecular Physics Department
71-103 Donath Street
400293 Cluj-Napoca, Romania

Abstract. Red blood cells (RBCs) in the presence of plasma proteins or other macromolecules have a tendency to form aggregates. Light-scattering technique was used to investigate the RBC aggregation process. A highly diluted suspension of RBCs was illuminated with a 632.8-nm HeNe laser. Angular-resolved measurements of light intensity scattered by an RBC suspension from a 200-μm thick optical glass cuvette during 10 min of their aggregation process were performed at 1 to 4 off-axis deg with a very high angular resolution, at hematocrits in the range of $3.5 \cdot 10^{-2}$ to 10^{-1}. The angular spreading of forward-scattered light at small angles during the RBC aggregation process was described in terms of a new, effective phase function model that has been used for fitting the experimental data. The aggregated RBCs' optical properties, such as effective scattering anisotropy and scattering cross section, were determined. The results were compared with prediction of Mie theory for equivolumetric spherical particles. The time dependence of the aggregates mean radius and of the mean number of cells per aggregate was also calculated. Last, the potential of the proposed technique (forward-scattering light technique) as a new quantitative investigation of cellular aggregation process was estimated. [DOI: 10.1117/1.2956658]

Keywords: red blood cells; aggregation; forward scattering; effective phase function; scattering cross section; effective scattering anisotropy; Mie theory.

Paper 07383SSR received Sep. 14, 2007; revised manuscript received Apr. 24, 2008; accepted for publication May 13, 2008; published online Jul. 18, 2008.

1 Introduction

The knowledge of the optical properties of human blood[1] (as a whole and also as components) plays an important role for many diagnostic and therapeutic applications in laser medicine and medical diagnostics. As a main component of blood, not only by their volume but also by their role, red blood cells (RBCs) can be easily collected, isolated, and handled. They have no internal macroscopic structure. Therefore, knowledge of the optical properties of RBCs in suspension, such as the scattering and absorption coefficients and the scattering phase function, is of crucial importance for the development of laser medicine. The dedicated literature, especially related to RBC optical properties, covers a diversity of aspects ranging from theoretical[2–8] and/or experimental[9–15] approaches to medical applications with diagnostic purposes.[16,17]

The morphology of RBC aggregation in whole blood and in RBC suspensions at rest and in shear flow is successfully studied by optical methods.[18–22] Previous studies of RBC aggregation have suggested that the aggregation process involves three steps. It starts with the formation of pairs from the cells that associate with each other side by side. Primary aggregates comprising only two adjacent cells develop further into linear aggregates of different lengths known as rouleaux.[23–25] These rouleaux are bound end-to-end and end-to-side. They form a three-dimensional (3-D) network that is tightened by cohesive forces into large dense aggregates (containing thousands of RBCs) separated by plasma layers. It is commonly accepted that such aggregation is mostly due to the nonspecific adsorption of the aggregating plasma proteins on the surfaces of adjacent RBCs. Nonetheless, there is evidence that protein adsorption is not the only mechanism for aggregation.[26,27]

Due to its importance in hemorheology, the RBC aggregation process has many approaches. Measurement of optical microscopy,[28] zeta sedimentation rate,[29] image analysis in a flow chamber,[30] ultrasound backscattering,[31,32] and photometry[19–22,33] are among the methods that have been employed to quantitatively study the aggregation. Despite the fact that RBC aggregation can be assessed using different techniques, two main approaches have been developed in the aggregometry. The first is based on the registration of light transmission through the studied blood layer in a cone-plate[21,22] or plate-plate[34] viscometer. The second approach is based on the registration of the backscattered light from a blood layer in a Couette-type viscometer.[19,20,35]

This paper reports the results of a quantitative investigation of the RBC aggregation process. The main goals of the

Address all correspondence to Cristian V. L. Pop, Natl. R&D Institute for Isotopic & Molecular Technologies, Molecular & Biophysics Dept., 71-103 Donath St., 400293 Cluj-Napoca, Romania. Tel: +40264584037 ext. 109; Fax: +40264420042; E-mail: cvl.pop@itim-cj.ro.

1083-3668/2008/13(4)/041308/8/$25.00 © 2008 SPIE

present study are to measure, with a very high resolution, the angular spreading of light forward scattered at small angles by RBCs in suspensions, at low hematocrits, during the aggregation process; to determine the behavior of aggregated RBCs' optical properties (scattering cross section and effective scattering anisotropy) during the aggregation process, comparing the measured data with the predictions of the new effective phase function model[3] and Mie theory; and to estimate the potential of the proposed technique (light forward-scattering technique) as a new method for quantitative investigation of the cellular aggregation process. In a previous published paper,[11] we made an accurate investigation of the angular spreading of light forward scattered at small angles by RBCs in suspensions, when all RBCs are singly dispersed.

2 Theoretical Aspects

2.1 *Forward-Scattered Light Distribution*

The theoretical approach using a red light at 632.8 nm is facilitated by the fact that RBCs have a very small absorption cross section[12] σ_a versus scattering cross section[11] σ_s ($\sigma_a \approx 0.2\ \mu m^2$, $\sigma_s \approx 68.4\ \mu m^2$, $\sigma_a/\sigma_s < 10^{-2}$), and consequently, almost all photons interacting with RBCs are scattered. Since the mean size of RBCs is roughly ten times larger than the wavelength of the incident radiation and the relative refractive index of the internal ($n_i \approx 1.40$) and external ($n_e \approx 1.33$) media is close to one ($n_r = n_i/n_e \approx 1.05$), the light is scattered in the forward direction in a narrow angular range, with the scattering process being extremely anisotropic. For these reasons, we measured the intensity of light scattered forward at small angles. Another reason, which is in fact more important, is that the photon flux can be described analytically in the small angle approximation[3] by an effective phase function $f_{eff}(\tau,\mu)$ (Henyey-Greenstein type),[3,11] if the two RBC parameters are known: the mean value of the scattering cross section σ_s and the scattering anisotropy g (the mean cosine of the scattering angle). This new effective phase function model[3,11] can be briefly described by the following equations:

$$\Phi_s = \phi_o(1-e^{-\tau}), \quad \frac{\phi_s(\tau,\mu)}{\phi_o} \approx (1-e^{-\tau}) f_{eff}(\tau,\mu), \qquad (1)$$

$$\tau = \mu d \approx \frac{\sigma_s}{v} H d,$$

$$f_{eff}(\tau,\mu) \approx \frac{1}{2}\frac{1-g_{eff}^2(\tau)}{[1-2g_{eff}(\tau)\mu + g_{eff}^2(\tau)]^{3/2}}, \qquad (2)$$

$$g_{eff}(\tau) = g^{\frac{(\tau-1)e^{\tau}+1}{e^{\tau}-\tau-1}},$$

where Φ_s is the total scattered photon flux, ϕ_o is the incident photon flux, τ is the optical depth, ϕ_s is the angular flux of the photons scattered in the direction given by the angle between the incident and the observation directions (axial symmetry setup), μ is the extinction coefficients ($\mu = \cos\theta$, where θ is the scattering polar angle), d is the sample thickness, v is the single RBC mean volume, and H is the hematocrit (volumic fraction of RBCs).

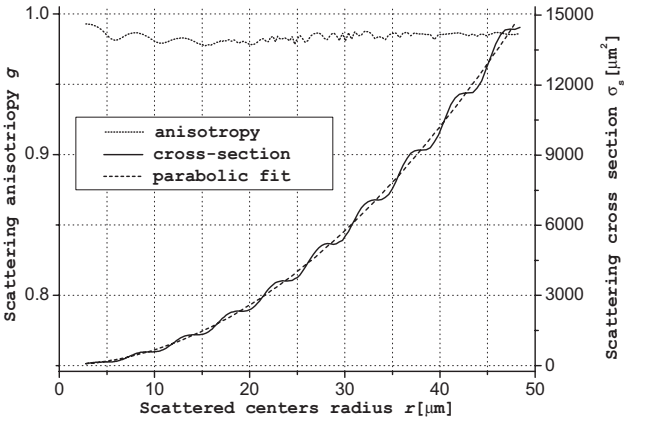

Fig. 1 Theoretical dependences by radius of scattering centers obtained from Mie theory for scattering anisotropy and scattering cross section. The scattering cross section is well-fitted by a parabolic function. All dependences start from $r_o = 2.78\ \mu m$ (the radius of a single RBC volume-equivalent sphere); below this value, there is no physical meaning for RBCs.

In Eq. (1), the attenuated flux of the unscattered photons is given by $\phi_o \cdot e^{-\tau}$, and the term $(1-e^{-\tau})$ shows in which way the total scattered light increases with optical depth, while the term $f_{\text{eff}}(\tau,\mu)$ describes the spatial distribution of the scattered light. The physical meaning of Eq. (2) is that the whole scattered volume exposed to the light beam can be modeled as a "macroscopic" particle having the same Henyey-Greenstein type phase function as for a single RBC but with the scattering anisotropy g replaced by τ-dependent effective anisotropy function $g_{eff}(\tau)$. The model described by Eqs. (1) and (2) is based on some approximations.[3,11] Its domain of validity is related to the attained desired accuracy and depends on the set of values for the g, θ, and τ parameters. The domain of validity depends strongly on τ and much less on θ and g. Further, it will be shown that the scattering anisotropy can be considered constant during the RBC aggregation process. Therefore, for a value of the scattering anisotropy $g = 0.979$ (experimental value for RBCs)[11] and a chosen angular domain $\theta = 1$ deg to 4 deg, the domain of optical depth will be $\tau \leqslant 10$ to ensure an accuracy higher than 95%.

The behavior for angular spreading of light scattered at small angles by a diluted suspension is revealed by three parameters: scattering anisotropy, scattering cross section, and concentration (expressed by hematocrit or scattering centers density). Based on Mie theory for equivolumetric spherical particles, the dependences of scattering anisotropy and scattering cross section by the radius of scattering centers can be obtained, as it is shown in Fig. 1. Two main observations arise from these dependences: in the first approximation, the scattering anisotropy can be considered independent of the scattering centers radius, and the scattering cross section has a quadratic dependence by radius of scattering centers.

The RBC aggregation process leads to a decrease of scattering centers per volume unit due to the fact that each aggregate becomes a new scattering center. Generally, in RBC suspensions, during the aggregation process, there is a heterogeneous distribution of aggregates having different number of cells and, consequently, different size. Moreover, the aggregation process being a dynamic one, the mean size

of aggregates, respectively the mean number of cells per aggregate, will increase in time. An other important fact is that in an RBC suspension, the hematocrit does not change during aggregation. As a result, the two ways to expres RBC suspension concentration, by hematocrit or scattering centers density, are not equivalent anymore.

2.2 *Working Hypothesis*

Due to the complexity of the RBC aggregation process, to find an accurate theoretical model that explains the angular distribution of scattered light by RBCs during the aggregation process is a real challenge. Nevertheless, there are few studies related to light scattered by aggregated RBCs,[36,37] but only for rouleaux consisting of two to eight cells. Consequently, to use the same approach for RBCs singly dispersed, some approximations of the RBC aggregation process were established. After the initial moment of time ($t=0$), when all RBCs are singly dispersed, at any other moment of time, the RBC aggregation process is ruled by our working hypothesis, as follows:

- All aggregates formed have the same number of cells N_a, represented by the mean number of cells per aggregate in real conditions.
- All aggregates are spherical,[28] each volume being proportional with N_a.
- The scattering cross section increases quadratically with the aggregate radius.
- Aggregates, once formed, do not break up (irreversible interaction).[28]

Under these hypotheses, we established the next equations:

$$V_a(r) = v(r/r_o)^3, \quad \sigma_s(r) = \sigma_{so}(r/r_o)^2, \tag{3}$$

$$\tau(r) = [\sigma_s(r)/V_a(r)]Hd = (r_o/r)\tau_o, \tag{4}$$

$$\text{with } \tau_o = (\sigma_{so}/v)Hd, \tag{5}$$

where V_a is the aggregate volume, r is the aggregate radius (represented by the aggregate mean radius in real conditions), and r_o is the radius of single RBC volume-equivalent sphere ($r_o=2.78$ μm for $v=90$ μm^3),[11,12] σ_{so} is the single RBC scattering cross section, and τ_o is the optical depth at the initial moment. In other words, the aggregate volume, scattering cross section, and optical depth become r-dependent functions during the RBC aggregation process. Further, based on Eq. (2), the effective anisotropy function g_{eff} becomes the r-dependent function g_{eff} $[\tau(r)]$. Obviously, the aggregates radius is a time-dependent parameter during RBC aggregation.

In conclusion, Eq. (4) shows that the increase of the aggregate mean radius leads to a decrease of suspension optical depth. Furthermore, during the aggregation process, the optical depth decreases with the power of the scattering centers density and increases with the cube of the radius, so the aggregate radius becomes the driving factor of the effective anisotropy parameter variation.

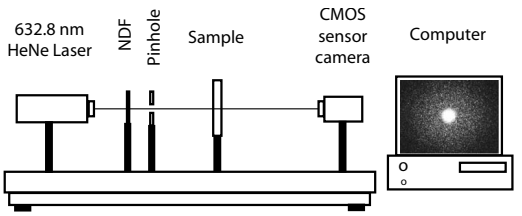

Fig. 2 Schematic diagram of the experimental setup used for angle-resolved measurements of light intensity scattered by RBC suspension at small angles.

3 Experimental Materials and Methods

3.1 *Preparation of Blood Samples*

Venous blood samples were obtained from healthy adult donors, with an age range of 25 to 47 years old and of either gender, via withdrawal into sterile vacuum tubes containing 3.8% natrium citrate. The RBCs were separated from the blood by centrifugation at 1200 g for 10 min and washed three times in an isotonic saline buffer (145 mM NaCl, 5 mM KCl, 5 mM HEPES, pH 7.4). Then, the washed RBCs were resuspended in autologous plasma with hematocrit values in the range of $3.5\cdot10^{-2} \leqslant H \leqslant 10^{-1}$ and used for light-scattering measurements and optical microscopy imaging. For all the experiments, the RBCs suspensions were stirred 3 min to disperse pre-existing RBC aggregates before placing them into a 200-μm-thick optical glass cuvette. All measurements were done at room temperature (21 ± 1 °C) and completed within 2 h after venipuncture.

3.2 *Experimental Setup*

The light source used was a 632.8-nm linearly polarized continuous-wave HeNe laser (JDS Uniphase, Model 1125P) with a power of 5 mW in TEM_{oo} mode. The beam diameter at $1/e^2$ was 0.81 mm, and the beam divergence 1 mrad. The laser beam was directed onto a 200-μm-thick optical glass cuvette (~20-μl volume) containing the sample of RBCs in suspension at rest. A complementary metal oxide aemiconductor (CMOS)[38] sensor monochrome camera (PixeLINK, Model PL-A741) with a resolution of 1280×1024 pixels at 27 fps was used to detect the small-angle scattered light. For monitoring the RBC aggregation process, the data were transferred in real time to a computer that captured an image (in bitmap file format) at each 10 s during 10 min, for each sample. The schematic diagram of the experimental setup it is shown in Fig. 2.

3.3 *Angular-Dependent Light Scattering Measurements*

Usually, the angular distribution of scattered light is detected by goniophotometric devices and can be performed on 180 deg with a resolution of 0.01 deg. Since our interest focuses on the domain of small scattering angles, the angular resolution was greatly improved by using a CMOS sensor camera as a detecting device. The angular detecting range in the forward direction was between 1 and 4 off-axis deg with a resolution of 3.125 millidegrees. The main difficulties that appear by when using coherent light sources are related to the speckled images given by the interference of scattered pho-

tons. In order to smooth the speckled images, the CMOS sensor camera was set up to 960×256 pixels at 100 fps, and each captured image was in fact obtained by averaging 500 frames. Due to the refraction effect, in order to obtain the correct scattering angles, the measured data were corrected to avoid the refractive index mismatch (internal media—plasma, and external media—air). Also, the relatively small contribution introduced by the nonspherical detecting surface of the CMOS sensor camera was corrected.

3.4 *Optical Microscopy Images Capture*

An upright optical microscope (Olympus, Model BX 51) linked to a computer via CCD color camera (Media Cybernetics, Model CoolSNAP-Pro CF) with a resolution of 1392 $\times$1040 pixels at 10 fps was used to capture images of RBC suspensions (one per min at 40$\times$ optical magnification), in the same conditions as the scattering measurements.

4 Results and Discussion

The angular-resolved measurements of light intensity scattered by an RBC suspension from a 200-μm-thick optical glass cuvette, during 10 min of the RBC aggregation process were performed at 1 to 4 off-axis deg, at hematocrits in the range of $3.5\cdot10^{-2}\leqslant H\leqslant10^{-1}$. In rest condition, the RBC aggregation process involves formation of 3-D large dense aggregates (containing thousands of RBCs) separated by plasma layers. This stage of aggregation is impossible in blood or suspended RBC layers as thin as those on the order of 25 μm to 40 μm,[1,19,21–23] typical for cone-plate or plate-pate aggregometers. For this reason, we selected a 200-μm-thick optical glass cuvette that is five or fifteen times thinner than the sample thickness of 1 mm used for backscattering[13,19] measurements or 3 mm for ultrasound[32] studies, respectively. The upper hematocrit limit ($H=10^{-1}$) is about five times smaller than the physiological value. It was chosen in order to keep the scattered light according to CMOS sensor sensibility, without exceeding the limit of the theory validity domain (see Sec. 2.1). Meanwhile, the lower hematocrit limit ($H=3.5\cdot10^{-2}$) was established in order to have enough cells closer to a realistic aggregation process. For the angular domain, the upper value was limited by the validity domain of the theory, and the lower value was chosen to avoid the transmitted (unscattered) photons. Due to the position of the laser beam on the cuvette, the very small significant sedimentation observed for upper hematocrits during measurement time (selected no longer than 10 min) does not influence the recorded data.

Figure 3 shows a few examples of the averaged speckle images (960×256 pixels) captured during the RBC aggregation process and the optical microscopy images for the lower and upper hematocrit limit at three moments in time. Looking at each series (H=const.) of averaged speckle images, there are obvious changes in the angular spreading of light intensity from a distribution almost isotropic at $t=0$ min to a high anisotropic one at $t=8$ min. This behavior is due to changes in the RBC suspension during the aggregation process, changes that can be observed in the optical microscopy images corresponding to the averaged speckle images. It is easy to observe in which way, starting from RBCs singly dispersed, the formatted rouleaux are bound end-to-end and end-to-side into 3-D, large, dense aggregates with a globular shape. Optical microscopy images were done for a supplementary confirmation of the RBC aggregate formation. They are somewhat unclear due to 200-μm depth of the optical glass cuvette but are similar to those reported in another study.[28] Unfortunately, this kind of unclear optical image acquired at a low rate 1/min cannot be used to make a computerized analysis for the distribution of the RBC population into aggregate size, similar to the 40-μm-depth samples reported in the literature.[23]

From the images captured at each 10 s and converted to a numerical matrix (256 gray levels), series of angular profiles (one for each hematocrit) giving the angular spreading of the scattered light intensity have been obtained during the RBC aggregation process. Considering for the RBC aggregation process the working hypothesis described in Sec. 2.2, the angular dependence of quasi-ballistic scattered photons from Eq. (2) was used as a fit function of the experimental data and also to determine the effective anisotropy parameter g_{eff}. The effective scattering anisotropy summarizes the information concerning the angular distribution of the scattered photons. Due to their graphic superposition, Fig. 4 shows only a few angular profiles of the scattered light intensity from the $H=10^{-1}$ series.

The decrease of the scattered light intensity with the increase of scattering angle θ, which is relatively well-fitted by a Henyey-Greenstein type phase function as in Eq. (2), depends parametrically on the sample hematocrit. For each investigated hematocrit, the scattering effective anisotropy behavior during the RBC aggregation process was obtained as a fit parameter of the angular-resolved measurements of scattered light intensity at different moments in time (Fig. 5). The t-dependent scattering effective anisotropy $g_{eff}(t)$ presents two regions: the first is characterized by a gradient that increases monotonically with the hematocrit, while for the second, the gradient is almost the same and has a very small value for all hematocrits. Each curve starts at different anisotropy of the scattering process, lower for higher hematocrit and vice versa, but all tend to have relatively the same value (around 0.972). In other words, the curves reveal the information concerning the angular redistribution of light intensity scattered by an aggregated RBC suspension. Moreover, based on our theoretical approach, the theoretical r-dependence of scattering effective anisotropy $g_{eff}(r)$ can be obtained from Eqs. (2), (4), and (5) for each studied hematocrit. The relation between the optical depth τ_o and hematocrit H given by the linear dependence $\tau_o=152\cdot H$, obtained from Eq. (5) for $d=200$ μm, $\upsilon=90$ μm^3, and $\sigma_{so}=68.4$ μm^2 was used. These theoretical dependences of scattering effective anisotropy $g_{eff}(r)$ are given in Fig. 6, where the curves start from $r_o=2.78$ μm (the radius of a single RBC volume-equivalent sphere); below this value, there is no physical meaning for RBC aggregates. The theoretical dependence of $g_{eff}(r)$ and the experimental dependence of $g_{eff}(t)$ were used to find the change of the aggregate mean radius in time during the RBC aggregation process for each investigated hematocrit (Fig. 7).

Another important parameter, the scattering cross section σ_s, which is a measure of the scattering efficiency, can be obtained from Eq. (3) if the time dependence of the aggregate mean radius is known. Figure 8 shows the time dependence of

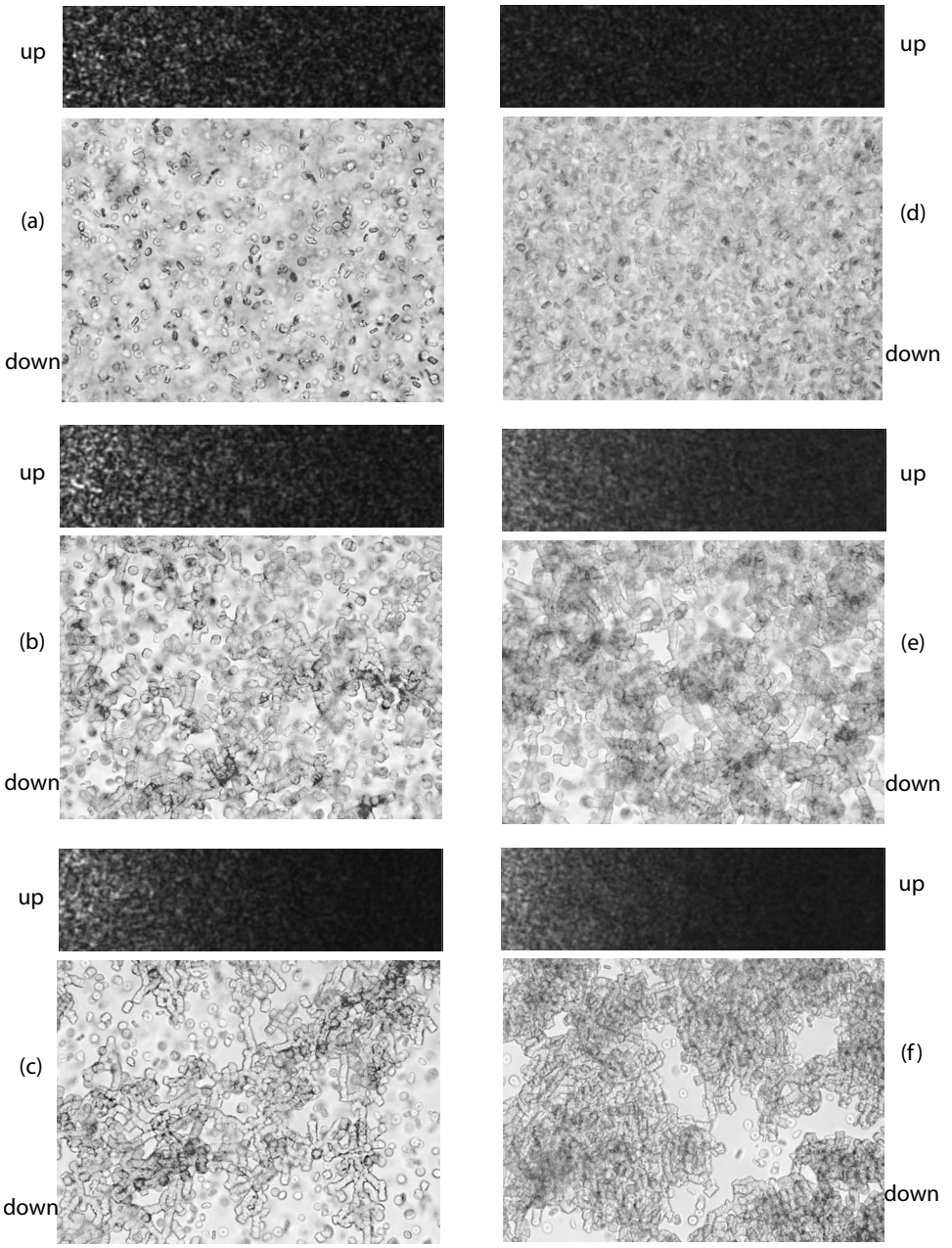

Fig. 3 The angular distribution (1 deg to 4 deg) of scattered light by aggregated RBCs in averaged speckle images (up—for each group of two images) and the associated optical microscopy images (down) during aggregation process at $H=3.5\cdot10^{-2}$ for: (a) 0 min, (b) 4 min, and (c) 8 min, and at $H=10^{-1}$ for same moments of time in (d), (e), and (f).

the scattering cross section σ_s during the RBC aggregation process at each studied hematocrit. The r-dependent scattering cross section during the RBC aggregation process from Eq. (3) was compared with the Mie theory prediction. This was done by using $\sigma_{s\ Mie}(r)=\sigma_{so\ Mie}(r/r_o)^2$ as a fitting function for the scattering cross section obtained from Mie theory. Here, $\sigma_{so\ Mie}$ is the scattering cross section at $r=r_o$; in other words, $\sigma_{so\ Mie}$ represents the scattering cross section for a single particle. Figure 9 gives the resulting data of the scattering cross section σ_s from all investigated hematocrits together with the Mie theory prediction. The values of scattering cross section obtained from experimental data for any hematocrit follow very well a parabolic function. At small aggregate mean radius, up to a value of 9 μm, our results are in agreement with Mie theory, but after that, the differences become significant. In Mie theory, the particles are spherical and identical, while the RBC aggregate particles are not identical and are far from spherical shape (see microscopy images in Fig. 3). For these reasons, our results for a radius above 9 μm are not in agreement with Mie theory. Moreover, by fitting the scattering cross section obtained from Mie theory, we can obtain $\sigma_{so\ Mie}=49.5\ \mu m^2$ at $r=r_o$, which is different from the experimental value[11] $\sigma_{so}=68.4\ \mu m^2$ used for calculating $\sigma_s(r)$. This difference is also a reason for the discrepancy between our results and the Mie theory prediction.

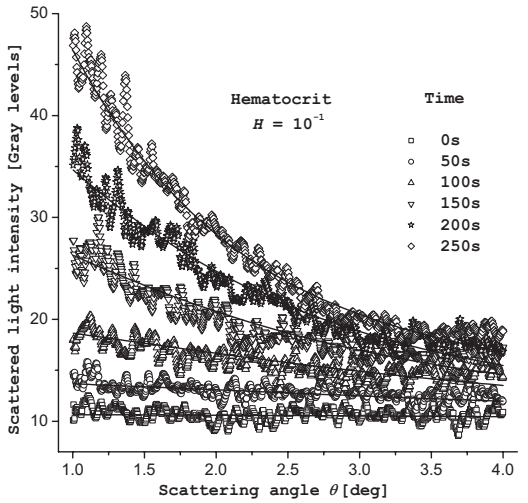

Fig. 4 Angle-resolved measurements for the averaged intensity of light scattered at small angles by RBCs suspended in plasma at different time moments during their aggregation process for $H=10^{-1}$ series, relatively well-fitted by a Henyey-Greenstein-type phase function, as in Eq. (2).

Based on our working hypothesis, which considers a spherical shape of RBC aggregates and the same number of cell per aggregate, N_a can be determined. At each moment in time, from the previously determined aggregate mean radius, taking into consideration $v=90\ \mu m^3$, the number of cells per aggregate was calculated (Fig. 10). From the time dependence of the number of cells per aggregate N_a (Fig. 10), we can define two different behavior regions. One of them, which starts with the first moment of the RBC aggregation process and lasts to about 3 min, is characterized by a slow increase of the N_a parameter. This behavior can be assigned to the first phase of the RBC aggregation process, where the aggregate is represented especially by the formation of rouleaux with different lengths. For this first region, our working hypothesis

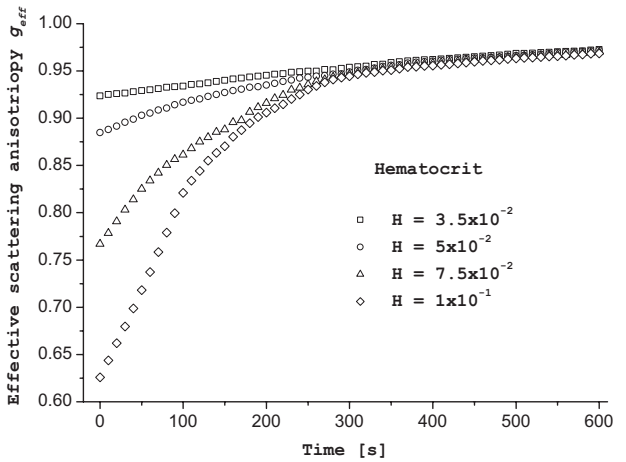

Fig. 5 The time dependences of the effective scattering anisotropy parameter during the first 10 min of the RBC aggregation process for each studied hematocrit. Each series of data (H=const.) was obtained as a fit parameter for angular profiles taken from angle-resolved measurements at each 10 s.

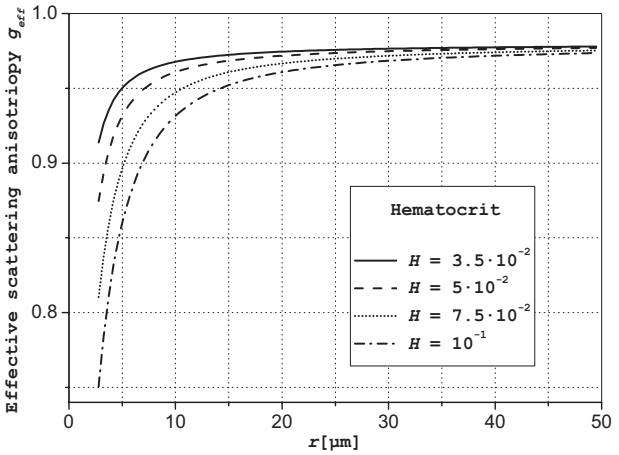

Fig. 6 The theoretical dependence of the effective scattering anisotropy parameter on one aggregate mean radius during the first 10 min of the RBC aggregation process for each studied hematocrit.

uses rough approximations. The other region is characterized by a high increase of the N_a parameter. This region reveals the second phase of the RBC aggregation process characterized by the formation of 3-D, large, dense aggregates with a globular shape, which are better approximated by our working hypothesis. There is a third region missing in which the N_a parameter tends to a plateau, due to our 10-min experimental limitation setup.

5 Conclusions

Our work was focused on following the main aspects of a quantitative investigation of the RBC aggregation process by light a scattering techniques at small angles:

- Angle-resolved measurements of the scattered light by aggregated RBCs in the range of small off-axis deflections to characterized redistribution of light intensity;
- Determination of the main ingredients, which ruled the investigated phenomenon of light scattered by aggregated

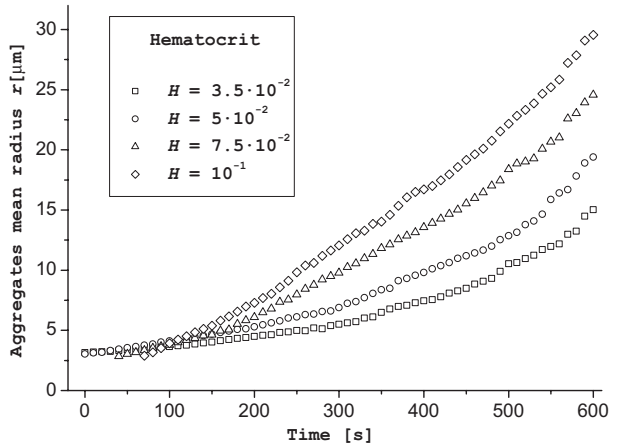

Fig. 7 The aggregate mean radius in time during the RBC aggregation process for each studied hematocrit. The values were obtained by comparing experimental t-dependent scattering effective anisotropy $g_{eff}(t)$ with theoretical r-dependent scattering effective anisotropy $g_{eff}(r)$.

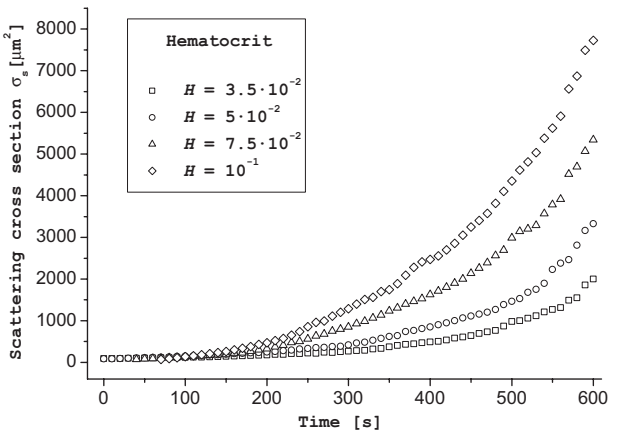

Fig. 8 The time dependence of scattering cross section σ_s during the RBC aggregation process for each studied hematocrit. The dependences were obtained based on the previously determined aggregate mean radius.

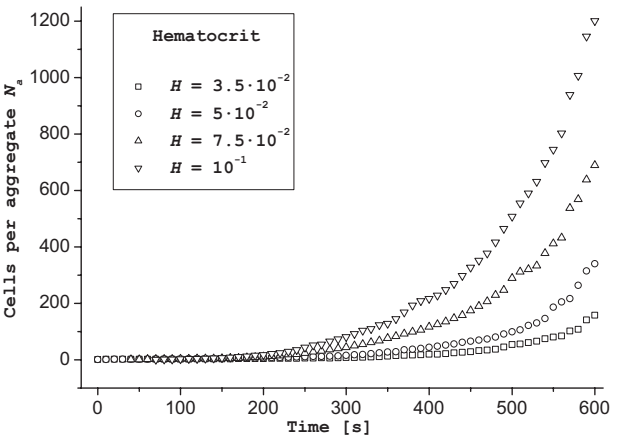

Fig. 10 The time dependence of the number of cells per aggregate N_a obtained from the previously determined aggregate mean radius, taking into consideration v=90 μm^3.

RBCs in suspension—the effective scattering phase function (more precisely, the associated effective scattering anisotropy) and the mean scattering cross section;

• Estimation of the proposed technique potential (light forward-scattering technique) as a new method for quantitative investigation of the cellular aggregation process.

RBCs in suspension at four different hematocrits were investigated, and the t-dependent scattering effective anisotropy $g_{eff}(t)$ was obtained from experimental measurement based on theoretical approach (new effective phase function model and our working hypothesis). This was compared with the theoretical prediction of r-dependent scattering effective anisotropy $g_{eff}(r)$ to find out the aggregate mean radius that quantitatively characterizes the RBC aggregation process. Further, the dependences of the mean scattering cross section in time and by the aggregate mean radius were determined. The dependences of the mean scattering cross section by the aggregate mean radius were compared with the prediction of Mie theory for equivolumetric spherical particles. Last, the time dependence of the mean number of cells per aggregate was calculated. This parameter can be used for a quantitative characterization of the RBC aggregate formation process as a two-phase process.

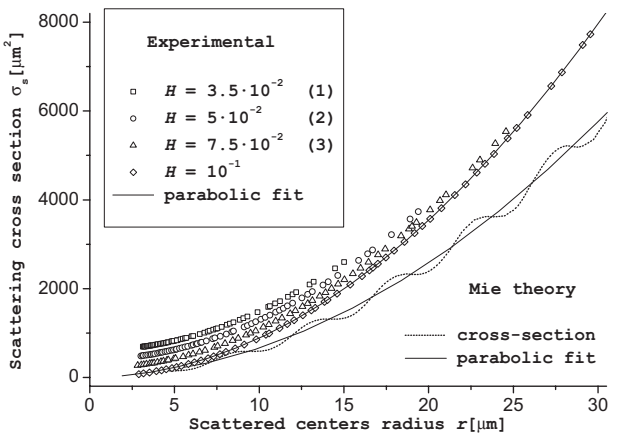

Fig. 9 The r-dependent scattering cross section during the RBC aggregation process obtained for all studied hematocrits and their parabolic fitting function. Due to graph superposition, three sets of our calculated data were shifted with: (1) +600 [μm^2], (2) +400 [μm^2], and (3) +200 [μm^2]. Comparatively, the Mie theory prediction is presented for the r-dependent scattering cross section and its parabolic fit.

The potential of the forward light-scattered techniques can be revealed even with our simple theoretical approach. Also, this can be achieved in the absence of a strong theoretical model for the RBC aggregation process and of a complementary one related to the scattered light intensity by RBCs during the aggregation process.

One can conclude that the light-scattering technique is a valuable alternative to classical aggregometric methods based on turbidimetric or backscattering measurements and can be used successfully in a quantitative investigation of the cellular aggregation process, due to its high sensitivity. The best results are obtained by detecting the off-axis scattered light at angles as small as possible. These results represent only the first several steps in a research field with a very high potential. Future work will be focused on the one hand, on the systematic investigation of several cases of relevant pathologies, and on the other hand, on the investigation of other cells with a relevant biomedical role, such as platelets. The final goal is to develop new, sensitive, and minimally invasive techniques for biological and medical diagnosis.

Acknowledgments

This work was supported by the Romanian Education, Research, and Youths Ministry, CEEX—VIASAN Program, Research Project No. 62/2005.

References

1. M. Friebel, A. Roggan, G. Müller, and M. Meinke, "Determination of optical properties of human blood in the spectral range 250 to 1100 nm using Monte Carlo simulations with hematocrit-dependent effective scattering phase functions," *J. Biomed. Opt.* **11**(3), 034021 (2006).
2. A. G. Borovoi, E. I. Naats, and U. G. Oppel, "Scattering of light by a red blood cell," *J. Biomed. Opt.* **3**(3), 364–372 (1998).
3. I. Turcu, "Effective phase function for light scattered by blood," *Appl. Opt.* **45**(4), 639–647 (2006).
4. S. V. Tsinopoulos and D. Polyzos, "Scattering of He-Ne laser light by

an average-sized red blood cell," *Appl. Opt.* **38**(25), 5499–5510 (1999).
5. A. M. K. Nilsson, P. Asholm, A. Karlsson, and A. Anderson-Engels, "T-matrix computations of light scattered by red blood cells," *Appl. Opt.* **37**(13), 2735–2748 (1998).
6. T. Wriedta, J. Hellmersb, E. Ereminab, and R. Schuh, "Light scattering by single erythrocyte: comparison of different methods," *J. Quant. Spectrosc. Radiat. Transf.* **100**(1–3), 444–456 (2006).
7. J. He, A. Karlsson, J. Swartling, and S. Andersson-Engels, "Light scattering by multiple red blood cells," *J. Opt. Soc. Am. A* **21**(10), 1953–1961 (2004).
8. A. Karlsson, J. He, J. Swartling, and S. Andersson-Engels, "Numerical simulations of light scattering by red blood cells," *IEEE Trans. Biomed. Eng.* **52**(1), 13–18 (2005).
9. A. Roggan, M. Friebel, K. Dörschel, A. Hahn, and G. Müller, "Optical properties of circulating human blood in the wavelength range 400–2500 nm," *J. Biomed. Opt.* **4**(1), 36–46 (1999).
10. A. N. Yaroslavsky, I. V. Yaroslavsky, T. Goldbach, and H.-J. Schwarzmaier, "Influence of scattering phase function approximation on the optical properties of blood determined from the integrating sphere measurements," *J. Biomed. Opt.* **4**(1), 47–53 (1999).
11. I. Turcu, C. V. L. Pop, and S. Neamtu, "High-resolution angle-resolved measurements of light scattered at small angles by red blood cells in suspension," *Appl. Opt.* **45**(9), 1964–1971 (2006).
12. M. Hammer, D. Schweitzer, B. Michel, E. Thamm, and A. Kolb, "Single scattering by red blood cells," *Appl. Opt.* **37**(31), 7410–7418 (1998).
13. A. H. Gandjbakhche, P. Mills, and P. Snabre, "Light-scattering technique for study of orientation and deformation of red blood cells in a concentrated suspension," *Appl. Opt.* **33**(6), 1070–1078 (1994).
14. G. J. Streekstra, A. G. Hoekstra, E. J. Nijhof, and R. M. Heethaar, "Light-scattering by red blood cells in ektacytometry: Fraunhofer versus anomalous diffraction," *Appl. Opt.* **32**(13), 2266–2272 (1993).
15. J. M. Steinke and A. P. Shepherd, "Comparison of Mie theory and the light scattering of red blood cells," *Appl. Opt.* **27**(19), 4027–4033 (1988).
16. J. D. Briers and S. Webster, "Laser speckle contrast analysis (LASCA): a nonscanning, full-field technique for monitoring capillary blood flow," *J. Biomed. Opt.* **1**(2), 174–179 (1996).
17. J. D. Briers, "Laser Doppler, speckle, and related techniques for blood perfusion mapping and imaging," *Physiol. Meas* **22**, R35-R66 (2001).
18. A. M. K. Enejder, J. Swartling, P. Aruna, and S. Andersson-Engels, "Influence of cell shape and aggregate formation on the optical properties of flowing whole blood," *Appl. Opt.* **42**(7), 1384–1394 (2003).
19. A. Priezzhev, O. M. Ryaboshapka, N. N. Firsov, and I. V. Sirko, "Aggregation and disaggregation of erythrocytes in whole blood: study by backscattering technique," *J. Biomed. Opt.* **4**(1), 76–84 (1999).
20. M. R. Hardeman, P. T. Goedhart, J. G. G. Dobbe, and K. P. Lettinga, "Laser-assisted optical rotational cell analyser (LORCA). I. A new instrument for measurement of various structural hemorheological parameters," *Clin. Hemorheol.* **14**(4), 605–618 (1994).
21. H. J. Klose, E. Volger, H. Brechtelsbauer, L. Heinich, and H. Schmid-Schönbein, "Microrheology and light transmission of blood. I. Photometric effects of red cell aggregation and red cell orientation," *Pflüg. Arch. Eur. J. Phy.* **333**(2), 126–139 (1972).
22. H. Schmid-Schönbein, K. A. Kline, L. Heinich, E. Volger, and T. Fischer, "Microrheology and light transmission of blood. II. The photometric quantification of red cell aggregate formation and dispersion in flow," *Pflüg. Arch. Eur. J. Phy.* **333**(2), 140–155 (1972).
23. G. Barshtein, D. Wajnblum, and S. Yedgar, "Kinetics of linear rouleaux formation studied by visual monitoring of red cell dynamic organization," *Biophys. J.* **78**(5), 2470–2474 (2000).
24. R. W. Samsel and A. S. Perelson, "Kinetics of rouleau formation. I. A mass action approach with geometric features," *Biophys. J.* **37**(2 I), 493–514 (1982).
25. R. W. Samsel and A. S. Perelson, "Kinetics of rouleau formation. II. Reversible reactions," *Biophys. J.* **45**(4), 805–824 (1984).
26. E. Evans and K. Buxbaum, "Affinity of red cell membrane for particle surfaces measured by the extent of encapsulation," *Biophys. J.* **34**(1), 1–12 (1981).
27. E. A. Evans, "Minimum energy analysis of membrane deformation applied to pipet aspiration and surface adhesion of red blood cells," *Biophys. J.* **30**(2), 265–284 (1980).
28. T. L. Fabry, "Mechanism of erythrocyte aggregation and sedimentation," *Blood* **70**(5), 1572–1576 (1987).
29. B. S. Bull and J. D. Brailsford, "The zeta sedimentation rate," *Blood* **40**(4), 550–557 (1972).
30. S. Chen, G. Barshtein, B. Gavish, Y. Mahler, and S. Yedgar, "Monitoring of red blood cell aggregability in a flow-chamber by computerized image analysis," *Clin. Hemorheol.* **14**(4), 497–508 (1994).
31. M. Boynard, J. C. Lelièvre, and R. Guillet, "Aggregation of red blood cells studied by ultrasound backscattering," *Biorheology* **24**(5), 451–461 (1987).
32. V. Rouffiac, P. Péronneau, J.-P. Guglielmi, M. Del-Pino, N. Lassau, and J. Levenson, "Comparison of new ultrasound index with laser reference and viscosity indexes for erythrocyte aggregation quantification," *Ultrasound Med. Biol.* **29**(6), 789–799 (2003).
33. H. Zhao, X. Wang, and J. F. Stoltz, "Comparison of three optical methods to study erythrocyte aggregation." *Clin. Hemorheol Microcirc* **21**(3–4), 297–302 (1999).
34. O. K. Baskurt, H. J. Meiselman, and E. Kayar, "Measurement of red blood cell aggregation in a "plate-plate" shearing system by analysis of light transmission," *Clin. Hemorheol Microcirc* **19**(4), 307–314 (1998).
35. M. Donner, M. Siadat, and J. F. Stoltz, "Erythrocyte aggregation: approach by light scattering determination," *Biorheology* **25**(1–2), 367–375 (1988).
36. S. T. Tsinopoulos, E. J. Sellountos, and D. Polyzos, "Light scattering by aggregated red blood cells," *Appl. Opt.* **41**(7), 1408–1417 (2002).
37. G. S. Stamatakos, N. K. Uzunoglu, and D. Yova, "An integral equation solution to the scattering of electromagnetic radiation by a system of two interacting triaxial dielectric ellipsoids. The case of a red blood cell rouleau," *J. Biomed. Opt.* **2**(3), 282–294 (1997).
38. D. Litwiller, "CMOS vs. CCD: maturing technologies, maturing markets," *Photonics Spectra* **39**(8), 54–59 (2005).